Distributions of inherent structure energies during aging

Ivan Saika-Voivod[1] and Francesco Sciortino[2]
[1]*Dipartimento di Fisica and Istituto Nazionale per la Fisica della Materia, Università di Roma La Sapienza, Piazzale Aldo Moro 2, I-00185 Roma, Italy*
[2]*Dipartimento di Fisica, Istituto Nazionale per la Fisica della Materia, and INFM Soft: Complex Dynamics in Structured Systems, Università di Roma La Sapienza, Piazzale Aldo Moro 2, I-00185 Roma, Italy*
(Received 22 January 2004; published 27 October 2004)

We perform extensive simulations of a binary mixture Lennard-Jones system subjected to a temperature jump in order to study the time evolution of fluctuations during aging. Analyzing data from 1500 different aging realizations, we calculate distributions of inherent structure energies for different aging times and contrast them with equilibrium. We find that the distributions initially become narrower and then widen as the system equilibrates. For deep quenches, fluctuations in the glassy system differ significantly from those observed in equilibrium. Simulation results are partially captured by theoretical predictions only when the final temperature is higher than the mode coupling temperature.

DOI: 10.1103/PhysRevE.70.041202 PACS number(s): 61.20.Lc, 64.70.Pf, 81.40.Cd

When a liquid is rapidly brought out of equilibrium, for example by an abrupt change in temperature T, it starts to age. The material properties change with the aging time t_w in the attempt to recover equilibrium at the new bath temperature T_b. This aging process can be visualized as a path in configurational space, that starts from a typical equilibrium configuration before the quench and which, at long times, should converge to an equilibrium configuration characteristic of T_b. When T_b is below the glass transition temperature, the aging dynamics never stops in the experimentally accessible time window, but becomes slower and slower on increasing t_w.

In recent years, several studies have revisited the physics of aging [1–4], attempting to associate the aging dynamics with a progressive decrease of the fictive (or effective) temperature T_f [5–9]. In these studies, the configuration of the aging system at time t_w is associated with a typical configuration explored by the equilibrium liquid at T_f. In this case, the aging dynamics can be modeled as a progressive thermalization of the system, quantified by the progressive decrease of T_f.

A convenient framework for analyzing the thermodynamics of supercooled liquids and aging dynamics in numerical simulations is provided by the inherent structure (IS) formalism [10]. In this framework, each configuration is associated with its closest local minimum, named IS, on the potential energy surface (PES) of the liquid. A formal thermodynamic description of the system can be developed with a proper modeling of the statistical properties of the PES, i.e., the distribution of the energy minima e_{IS} and of their basins of attraction [10,11]. It has been shown that in equilibrium supercooled states, the probability density $P(e_{IS},T)$ of exploring a minimum of depth e_{IS} is approximately Gaussian, with a T-independent variance and with an average $\overline{e_{IS}}$ which decreases monotonically with T [12–14]. In the IS approach, the aging dynamics can be visualized as the progressive exploration of deeper and deeper minima, and a connection between aging and equilibrium configurations can be made by comparing properties of the explored basins.

Experimental studies of glass forming materials [4,15] and recent numerical simulations [16] have called attention to the fact that aging systems, especially for deep quenches, may not be associated with a single T_f, i.e., cannot be uniquely associated with a liquid configuration, calling for a further development of the present theories. In this paper, we bring the level of comparison between equilibrium and aging to a much more detailed level, by studying fluctuations around the average properties. We show that the fluctuations frozen in the glass depend on the thermal history and are significantly different from the fluctuations characteristic of the liquid state.

We perform molecular dynamics (MD) simulations of $N=1000$ particles in a cubic box of length $L=9.4$, for the well characterized Kob-Andersen binary-mixture Lennard-Jones (LJ) model [17], for which the mode coupling transition has been estimated at $T_x=0.435$. We employ the Nosé-Hoover thermostat with parameters chosen so that the kinetic energy thermalizes in a time between 300 and 1000 time steps. Time is reported here in number of MD time steps, each of which is $0.01t_0$ [18]. We calculate the probability density $P(e_{IS},t_w)$ of finding the liquid at a given time t_w in a basin of energy e_{IS}, as the system responds to a sudden lowering in T. To this end, we perform an ensemble of 1500 independent MD runs, each for 10^6 steps. The temperature is switched from the initial equilibrium temperature T_i to the new T_b at $t_w=0$. For each MD run we select configurations at 35 different t_w, logarithmically spaced. We perform a conjugate-gradient quench on each configuration to obtain the associated IS. Diagonalization of the Hessian matrix evaluated at the IS provides the eigenfrequencies $\{\omega_i\}$. Thus for each studied t_w we produce an ensemble of 1500 IS's. We study five different T jumps, with sets of $(T_i \rightarrow T_b)$, including $(0.55 \rightarrow 0.466)$, $(0.6 \rightarrow 0.1)$, $(0.8 \rightarrow 0.25)$, $(0.8 \rightarrow 0.446)$, and $(0.8 \rightarrow 0.6)$.

In Fig. 1 we plot $P(e_{IS},t_w)$ for the $(0.8 \rightarrow 0.446)$ run, as well as the corresponding equilibrium distributions $P(e_{IS},T)$ at T_i and T_b. The figure shows that distributions initially become narrower (equivalently taller), then broader again on

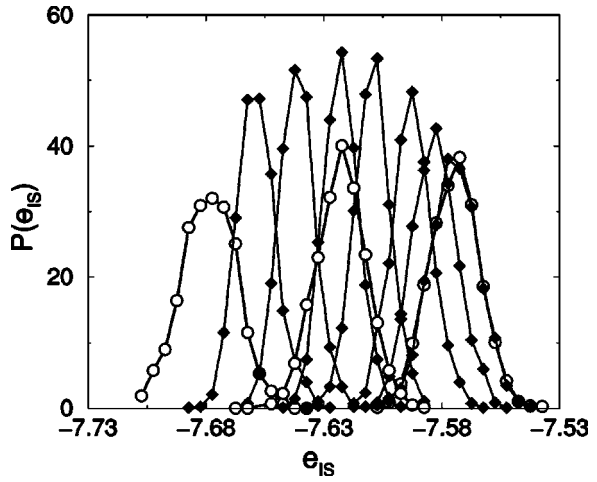

FIG. 1. Distributions of e_{IS} during aging. Histograms (of unit area) showing $P(e_{IS},t_w)$ (filled diamonds) for an ensemble of aging systems with $T_i=0.8$ and $T_b=0.446$ with $t_w=542$, 3405, 7482, 21372, 46954, 174338, and 841500 from right to left. Also shown are equilibrium distributions $P(e_{IS},T)$ (open circles) for $T=0.8$, 0.55, and 0.446 from right to left.

approaching equilibrium. Figure 2 shows the average e_{ag} and the standard deviation σ_{ag} of the distributions as functions of t_w. In the cases where $T_b > T_x$, the variance, which by construction at $t_w=0$ coincides with the equilibrium variance, first decreases and then relaxes towards the equilibrium value. For $T_b < T_x$, within the studied time window, we only observe the narrowing. We also evaluate the skewness, though we cannot discern any trend outside of statistical noise.

Next we attempt to compare the fluctuations observed in aging with theoretical predictions. In equilibrium, the Helmholtz free energy per particle of the liquid can be written as [10,12]

$$F = e_{IS} - TS_c(e_{IS}) + f_{vib}(e_{IS},T), \tag{1}$$

where $f_{vib}(e_{IS},T)$ is the free energy of a basin, averaged over all basins of depth e_{IS}, and $S_c(e_{IS})=N^{-1}k_B \ln \Omega(e_{IS})$ is the configurational entropy. $\Omega(e_{IS})$ counts the number of basins of energy e_{IS}. In the Gaussian-harmonic approximation (GHA) [19], one assumes that S_c and f_{vib} are quadratic in e_{IS}. In the GHA, $P(e_{IS},T)$ is Gaussian with a T-independent variance, i.e.,

$$P(e_{IS},T) = \frac{1}{\sqrt{2\pi\sigma_P^2}} \exp\left[-\frac{(e_{IS} - \overline{e_{IS}}(T))^2}{2\sigma_P^2} \right], \tag{2}$$

where the T dependence of $\overline{e_{IS}}$ and the variance σ_P^2 are expressed in terms of the statistical properties of the PES [the variance σ_c^2 and the average energy E_0 of $\Omega(e_{IS})$] and of the parameters connecting depth and shape of the basins (b and c) [20,21]. More precisely, $\overline{e_{IS}}(T)=(E_0 - b\sigma_c^2)/(1+2c\sigma_c^2) - T^{-1}\,\sigma_c^2/(1+2c\sigma_c^2)$, and $\sigma_P^2=N^{-1}\sigma_c^2/(1+2c\sigma_c^2)$. Below $T=0.6$, the GHA provides a good description of the numerical data [12,14], enabling us to estimate σ_c^2, E_0, b, and c.

In the nonequilibrium case, recent theoretical approaches suggest that the free energy can be written as

$$F = e_{IS} - T_f S_c(e_{IS}) + f_{vib}(e_{IS},T_b), \tag{3}$$

where S_c is weighted by T_f [6,8,22,23]. The introduction of T_f modifies Eq. (2) to yield a nonequilibrium probability density, in the GHA,

$$P(e_{IS},T_f(t_w),T_b) = \frac{1}{\sqrt{2\pi\sigma_{ag}^2}} \exp\left[-\frac{(e_{IS} - e_{ag})^2}{2\sigma_{ag}^2} \right], \tag{4}$$

where e_{ag} and σ_{ag} are given by

$$e_{ag} = \frac{E_0 T_f - \sigma_c^2 - \sigma_c^2 T_b b}{2c\sigma_c^2 T_b + T_f}, \tag{5}$$

and

$$\sigma_{ag}^2 = N^{-1}\left(2c + \frac{1}{\sigma_c^2}\frac{T_f}{T_b} \right)^{-1}. \tag{6}$$

Note that the theory predicts a gradual increase of the variance on increasing t_w, i.e., on approaching equilibrium (decreasing T_f).

The theoretical predictions for the relation between e_{ag} and σ_{ag}, parametric in T_f, are shown in Fig. 3(a). In Fig. 3(b) we show the evolution of the same quantities as calculated from the aging runs. In the simulation data, at short t_w, the system possesses by construction a distribution of IS energies identical to that of the starting T, and hence it is not surprising that the numerical results initially differ from the value predicted by Eq. (6). For longer times, i.e., for lower e_{IS} values, a region where the variance increases is indeed observed, but only for quenches above T_x. The magnitude of change in the variance predicted by the theory is significantly smaller than the one observed in simulation. Even in the case $(0.55 \rightarrow 0.466)$, where the starting T is such that the GHA should hold the best, the observed narrowing falls outside the

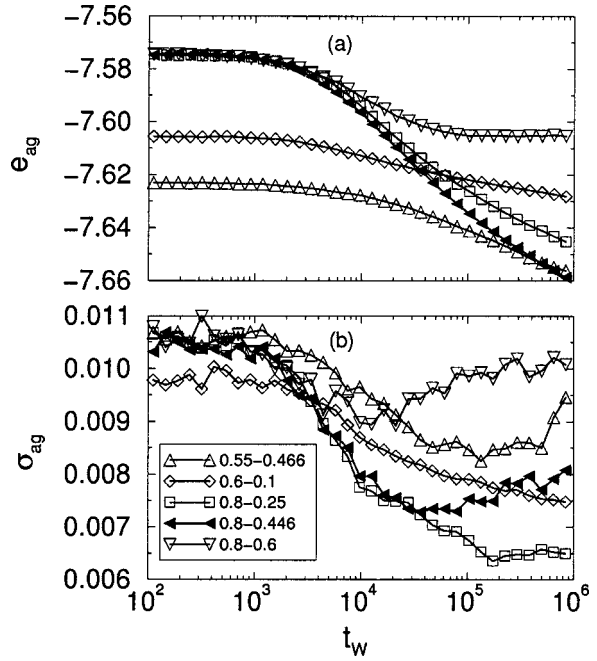

FIG. 2. Time evolution of the average e_{ag} (a) and of the standard deviation σ_{ag} (b) of the inherent structure energy distribution $P(e_{IS},t_w)$. Legend indicates the corresponding T_i and T_b values.

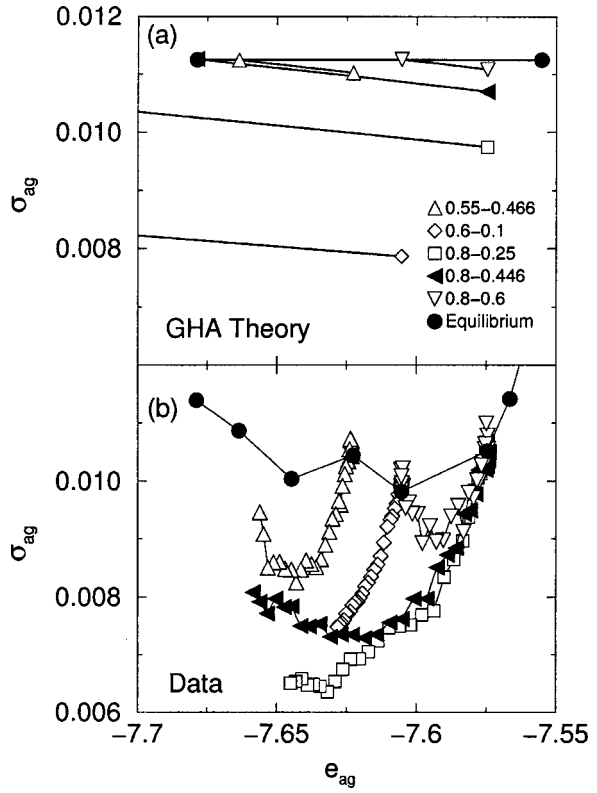

FIG. 3. Relationship between σ_{ag} and e_{ag} during aging. The legend indicates T_i and T_b. Panel (a) shows the theoretical predictions based on the GHA, using the landscape parameters calculated fitting equilibrium data [21]. Panel (b) shows MD data. Filled circles indicate equilibrium values.

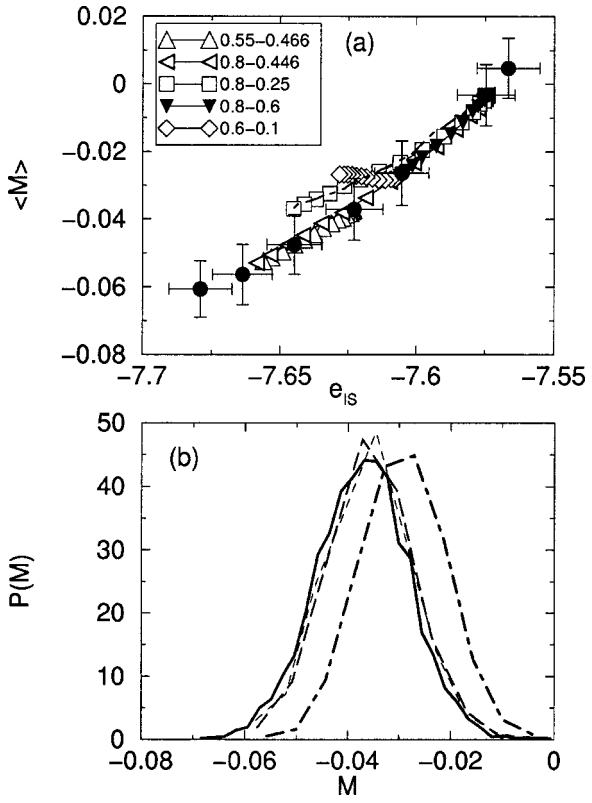

FIG. 4. Vibrational properties of basins as a function of e_{IS}. Panel (a) shows $\langle M\rangle_{eq}(e_{IS})$ (filled circles, bars indicating standard deviations) and aging ensemble averages $\langle M\rangle_{ag}(e_{IS})$. For the dot-dash line we use a binning procedure to determine $M(e_{IS})$ from all basins regardless of t_w during aging for the $(0.8\rightarrow0.25)$ run. Panel (b) shows the equilibrium $P(M)$ for $T=0.55$ (solid line), and for the case where all basins with energy $\overline{e_{IS}}(T=0.55)\pm0.002$ are used (short dash); and for the aging runs $(0.8\rightarrow0.446)$ (long dash) and $(0.8\rightarrow0.25)$ (dot dash), also binning the energy.

uncertainty arising from modeling the equilibrium distributions, as well as from numerical errors.

An implicit assumption in the theory is that, during aging, the liquid explores configurations typical of equilibrium [24] and hence that the landscape parameters derived from the equilibrium study can be used to calculate the out-of-equilibrium distributions. Previous work has shown that this is not necessarily so [25]. Here we analyze our extremely large database of inherent structures in equilibrium and in aging to address the question of whether the basin curvature during aging differs from the equilibrium case. The quantity $M\equiv N^{-1}\Sigma_{i=1}^{3N-3}\ln(\hbar\omega_i/\epsilon_{AA})$ constitutes a good indicator of the curvature of a single basin in the harmonic approximation [24,25]. In Fig. 4(a) we plot average values $\langle M\rangle_{eq}(e_{IS})$ and $\langle M\rangle_{ag}(e_{IS})$ for equilibrium and aging runs. This plot shows that for all aging experiments with $T_b>T_x$, the e_{IS} dependence of M is the same in equilibrium and in aging, and hence that the aging liquid explores basins the shape of which is the same as the one explored in equilibrium. In contrast, for $T_b<T_x$, the aging system explores basins of different shape. In the $(0.8\rightarrow0.25)$ case, the system begins to explore basins of higher M relative to equilibrium values near $e_{IS}\approx-7.6$. In the deep quench $(0.6\rightarrow0.1)$ case, the system stays in basins of roughly constant f_{vib}. It is as though the system explores basins of lower energy, but not of correspondingly lower f_{vib}. To discern the origins of the differences in basin sampling in aging and equilibrium, we calculate the distribution of M, $P(M)$, for four different cases [Fig. 4(b)]. More specifically, we want to assess if differences in $\langle M\rangle$, at the same average e_{IS} value, arise from differences in the distributions of sampled e_{IS} or if they arise from intrinsic differences in sampled basin shapes. For this reason we show, together with the equilibrium case for $T=0.55$ (for which $\overline{e_{IS}}=-7.6228$), the $P(M)$ for basins of depth $e_{IS}=-7.6228\pm0.002$, explored in the shallow $(0.8\rightarrow0.446)$ and deep $(0.8\rightarrow0.25)$ quenches (independent from t_w) and basins explored in equilibrium (independent from T). Data in Fig. 4(b) show that the equilibrium $P(M)$ coincides with the distribution evaluated from all sampled basins with depth equal to $e_{IS}=-7.6228$. It also coincides with the distributions evaluated during aging in the $T_b>T_x$ runs. But it does not coincide with the distributions evaluated during aging in the $T_b<T_x$ case. Hence, differences between equilibrium and aging cannot be ascribed to the nonlinear dependence of M on e_{IS}. We conclude that in aging runs with $T_b<T_x$ the system explores narrower basins (higher M) as compared to equilibrium.

The results reported in this paper provide high quality data for the evolution of the energy distribution in aging, for several different aging scenarios, and hence provide an im-

portant starting point for a detailed master equation description [26–29] of the dynamics in configuration space. In our simulations, when $T_b > T_x$, we find that the distribution initially narrows during aging, broadening again as the system reequilibrates. We also find that the system samples configurations which are typically explored in equilibrium. In this T range, a description of the aging dynamics via a master equation is feasible, provided equilibrium properties are fully characterized. By contrast, when $T_b < T_x$, we only observe the narrowing of the distribution. Furthermore, the vibrational states explored during aging differ from the equilibrium ones. Hence, while the PES approach retains its validity in the thermodynamic description of equilibrium properties of supercooled liquids, a thermodynamic extension of this approach to aging is not straightforward.

We note that the present out-of-equilibrium theory, which is built on the hypothesis that states explored in aging are the same as those explored in equilibrium, predicts only broadening associated with the approach to equilibrium. One could question the role of the GHA in the discrepancy between theory and simulation. In this respect we note that the case $(0.55 \rightarrow 0.466)$ should be only weakly affected by the GHA approximation. Indeed, T is sufficiently low to minimize anharmonic effects, and high enough to avoid effects due to non-Gaussianity of the density of states. Moreover, the vibrational states explored during aging are the same in this case. Hence, the GHA is not the dominant origin of the observed deviations.

In summary, a theory based on a single T_f may only apply to the $T_b > T_x$ case. We also stress that the results reported suggest that fluctuations in arrested states (which on the time scale of simulation correspond to $T_b < T_x$) depend on the previous thermal history [26,28]. Glasses with the same average values may strongly differ in their frozen fluctuations. For deep quenches, the fluctuations frozen in the glass are significantly different from the fluctuations experienced in the liquid state, a feature which could explain the crossover effect [4,16,28] and the failure of the theories based on one T_f. Finally, we note that the decrease of the variance at short times (as shown in Fig. 2), suggests that the initial aging dynamics—which may well be the only one accessible on the observation time scale for deep quenches—acts in the direction of increasing the differences between the equilibrium liquid and glass distributions.

We thank SHARCNET for computing resources. I.S.-V. acknowledges NSERC for financial support. We acknowledge support from MIUR Cofin 2002 and Firb and INFM Pra GenFdt.

[1] A. Q. Tool, J. Am. Ceram. Soc. **29**, 240 (1946).
[2] J. Brawer, *Relaxation in Viscous Liquids and Glasses* (The American Ceramics Society, Columbus, OH, 1985).
[3] G. W. Scherer, *Relaxation in Glass and Composites* (Wiley, New York, 1986).
[4] G. B. McKenna, in *Comprehensive Polymer Science*, edited by C. Booth and C. Price (Pergamon, Oxford, 1989), Vol. 2, pp. 311–362.
[5] L. F. Cugliandolo *et al.*, Phys. Rev. E **55**, 3898 (1997).
[6] S. Franz and M. A. Virasoro, J. Phys. A **891**, 891 (2000).
[7] Th. M. Nieuwenhuizen, Phys. Rev. Lett. **80**, 5580 (2001); L. Leuzzi and Th. M. Nieuwenhuizen, Phys. Rev. E **64**, 011508 (2001).
[8] F. Sciortino and P. Tartaglia, Phys. Rev. Lett. **86**, 107 (2001).
[9] S. Mossa *et al.*, Eur. Phys. J. B **30**, 351 (2002); J. Phys.: Condens. Matter **15**, S351 (2003).
[10] F. H. Stillinger and T. A. Weber, Phys. Rev. A **25**, 978 (1982); Science **225**, 983 (1984); F. H. Stillinger, *ibid.* **267**, 1935 (1995).
[11] The set of particle configurations which map onto the same local minimum via a path of steepest descent form a so-called basin.
[12] F. Sciortino *et al.*, Phys. Rev. Lett. **83**, 3214 (1999).
[13] A. Heuer and S. Büchner, J. Phys.: Condens. Matter **12**, 6535 (2000).
[14] S. Sastry, Nature (London) **409**, 164 (2001).
[15] A. J. Kovacs, Fortschr. Hochpolym.-Forsch. **3**, 394 (1963).
[16] S. Mossa and F. Sciortino, Phys. Rev. Lett. **92**, 045504 (2004).
[17] W. Kob and H. C. Andersen, Phys. Rev. E **51**, 4626 (1995); **52**, 4134 (1995).
[18] Here $t_0 = \sqrt{(m\sigma_{AA}^2/48\epsilon_{AA})}$, where m is the particle mass, and σ_{AA} and ϵ_{AA}, which enter in the LJ potential, are the units of length and energy.
[19] E. La Nave *et al.*, J. Phys.: Condens. Matter **15**, S1085 (2003).
[20] In the harmonic approximation, $f_{vib}(e_{IS},T) = k_B T[\ln\langle e^M\rangle - 3(1 - 1/N)\ln(k_B T/\epsilon_{AA})]$, where $M = N^{-1}\Sigma_{i=1}^{3N-3} \ln(\hbar\omega_i/\epsilon_{AA})$, N is the number of particles, and k_B is the Boltzmann constant.
[21] By fitting $\overline{e_{IS}}(T)$ and $\langle M\rangle = \ln\langle e^M\rangle = a + be_{IS} + ce_{IS}^2$, we obtain $a = 166.34$, $b = 43.07$, $c = 2.787$, $E_0 = -6.596$, and $\sigma_c^2 = 0.43$.
[22] E. La Nave *et al.*, Phys. Rev. E **68**, 032103 (2003).
[23] T. S. Grigera *et al.*, Phys. Rev. B **70**, 014202 (2004).
[24] W. Kob *et al.*, Europhys. Lett. **49**, 5906 (2000).
[25] S. Mossa *et al.*, Philos. Mag. B **82**, 695 (2002).
[26] J. C. Dyre, Phys. Rev. Lett. **58**, 792 (1987); Phys. Rev. B **51**, 12276 (1995).
[27] C. Monthus and J.-P. Bouchaud, J. Phys. A **29**, 3847 (1996); B. Rinn *et al.*, Phys. Rev. Lett. **84**, 5403 (2000); R. A. Denny *et al.*, *ibid.* **90**, 025503 (2003).
[28] E. M. Bertin *et al.*, J. Phys. A **36**, 10701 (2003).
[29] T. Keyes *et al.*, Phys. Rev. E **66**, 051110 (2002).